Received: 21 May 2020 | Revised: 21 September 2020 | Accepted: 27 September 2020

DOI: 10.1002/app.50074

ARTICLE

Applied Polymer SCIENCE WILEY

Synthesis of β-myrcene-based macroporous nanocomposite foams: Altering the morphological and mechanical properties by using organo-modified nanoclay

Burcu Kekevi[1] | **Emine Hilal Mert**[2]

[1]Yalova Community College, Material and Material Processing Department, Yalova University, Yalova, Turkey

[2]Faculty of Engineering, Department of Polymer Materials Engineering, Yalova University, Yalova, Turkey

Correspondence
Burcu Kekevi, Yalova Community College, Material and Material Processing Department, Yalova University, Yalova, Turkey.
Email: bkekevi@yalova.edu.tr

Emine Hilal Mert, Faculty of Engineering, Department of Polymer Materials Engineering, Yalova University, Yalova, Turkey.
Email: hmert@yalova.edu.tr

Abstract

Organo-modified nanoclay incorporated high internal phase emulsions (HIPEs) were successfully used for the preparation of macroporous nanocomposite foams. Due to the aim of obtaining mechanically improved foams, HIPEs were prepared by using a monomer mixture composed of β-myrcene and ethylene glycol dimethacrylate. Accordingly, two groups of macroporous nanocomposite foams were synthesized depending on the nanoclay type. The morphological analysis demonstrated that the pore openness of the resulting nanocomposites were significantly improved due to the decrease in the average cavity size and increase in the interconnected pore size. In terms of mechanical properties, it was found that filling 1 wt% of nanoclay which is surface modified by hydrogenated tallow lead to a 33% of increment in the compression modulus, as compared to the neat foam. However, loading 5 wt% of nanoclay having octadecylamine and aminopropyltriethoxysilane surface groups caused only 11% of increment in the compression modulus, as compared to the neat foam.

KEYWORDS

crosslinking, foams, mechanical properties, morphology, porous materials

1 | INTRODUCTION

Poly(high internal phase emulsion)s (polyHIPEs) are an important class of macroporous polymer foams offerring the advantage of hierarchical porosity accompanied with highly permeable structure.[1–3] PolyHIPEs are usually prepared by the polymerization of the monomer containing phase of HIPEs, which are concentrated emulsions consisting of a high volume fraction of internal phase. The volume fraction of the internal phase of a HIPE is greater than 0.74 and can be increased up to 0.99. Thus, creation of the highly porous structure is mainly dependent on the internal phase ratio.[1–6] Upon the polymerization of the monomer containing phase a continuous polymer film is formed and during this process internal phase droplets remain in between the polymer film. By the removal of droplet phase after polymerization, hierarchical open porous structure is formed.[1–6]

PolyHIPEs exhibits two-stage porosity composed of primary cavities (macropores) interconnected with each other by secondary pores (interconnected pores).[4,7] As a result of the high presence of macropores mechanical strength of polyHIPEs is rather low and this is one of the major disadvantage to overcome.[6,8–11] On the other hand, since ultimate polyHIPE properties are mainly dependent on the precursor-HIPEs, experimental parameters related to emulsion preparation should also be considered.[6] Emulsion stability is another important concern on polyHIPEs. Since emulsions are thermodinamically unstable, the choice of the components of HIPEs, such as monomer(s), emulsifying agent(s) or in some cases nanoparticles have great importance.[12,13] Considering the emulsion stability, hydrophobic

monomers, such as styrene and divinylbenzene, are the most used kinds in polyHIPE synthesis. However, polystyrene-based polyHIPEs usually suffer from chalkiness and brittleness.[6,10,14,15] In addition, limited source of petroleum-based monomers is also another disadvantage that cannot be ignored. To overcome these drawbacks, several approaches, such as replacing monomer system,[11,15,16] using a stress reducer monomer,[9,10] or incorporating reinforcement nanoparticles,[8,9,11,17,18] have been used by scientists. In this respect, incorporating nanoclay particles in the polymer matrix have been attracting much of interest while there several studies addressing the preparation of polyHIPE/nanoclay composites and nanocomposites have been reported.[17,19–25] Previous studies showed that incorporating nanoparticles in the polyHIPE matrix brings additional advantages depending on the nature of the choosen nanoparticles. For instance, nanoparticles may provide additional sites for crosslinking,[2,5,20] add functionality to the polymer,[12,13] and improve morphological, thermal, and mechanical properties.[11,17–27]

Hierarchical porosity, permeability, and low density of polyHIPEs enable these materials to find application in many areas, such as energy storage, adsorption, and tissue engineering.[2–5] PolyHIPEs with various chemistries and functionality can be synthesized with tuned properties for a wide range of applications. At this respect, nanoclay-incorporated polyHIPEs are coming forward within emulsion templated foams not only because of their improved morphology and mechanical strength, but also the advantages of providing additional benefits in terms of application. In this frame, acrylate-based polyHIPEs obtained by the addition of various amounts of surface-modified montmorillonite (MMT) was used for the adsorption of methyl violet 2B by Yüce et al.[23] Mert et al. used Spirulina (Sp) microalgae-modified MMT for the synthesis of adsorbent polystyrene polyHIPEs for use in removing dye molecules.[25] More recently, polystyrene-based n-hexadecane/polyHIPE containing surface-modified MMT has been successfully used by Mert as a form-stable phase change material.[27] Although abovementioned studies reveal the advantages of incorporating nanoclay, the resulting polyHIPE materials still suffer from the insufficiency of mechanical or morphological properties. Since acrylates are relatively hydrophilic monomers having different degrees of water solubility, phase inversion, and droplet coalescence processes are determinative for pore morphology.[23] On the other hand, styrene is a highly hydrophobic monomer and emulsion destabilization processes are mostly eliminated during the polymerization of styrene-based HIPEs. Thereby, these foams usually exhibit a highly open and hierarchical morphology. However, brittleness and chalkiness of polystyrene polyHIPEs are their major drawback.[6,10,11,16,18]

The present study deals with the synthesis of macroporous polyHIPE/nanoclay nanocomposite foams by using two different organo-modified commercial MMT via HIPE templating. For this purpose, since it is a naturally occuring feedstock, and has various benefits, such as producing crosslinked polymer matrix and improving mechanical strength by providing isoprene like building blocks, β-myrcene was used as monomer in the continuous phase.[28–30] Moreover, ethylene glycol dimethacrylate (EGDMA) was chosen as a crosslinker in order to increase the polymer chain flexibility. By using the mixture of β-myrcene and EGDMA the polarity of the oil phase was also balanced.[30] It was also shown that nanoclay incorporation can be successfully used for tailoring the polyHIPE morphology and as well as the compressive properties. In addition, it was demonstrated by using two different types of organo-modified MMT that the organo-modifier groups have a significant influence on the final properties. The findings of this study

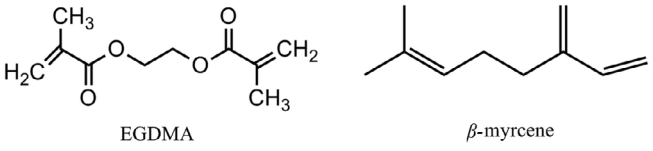

FIGURE 1 Chemical structures of monomers

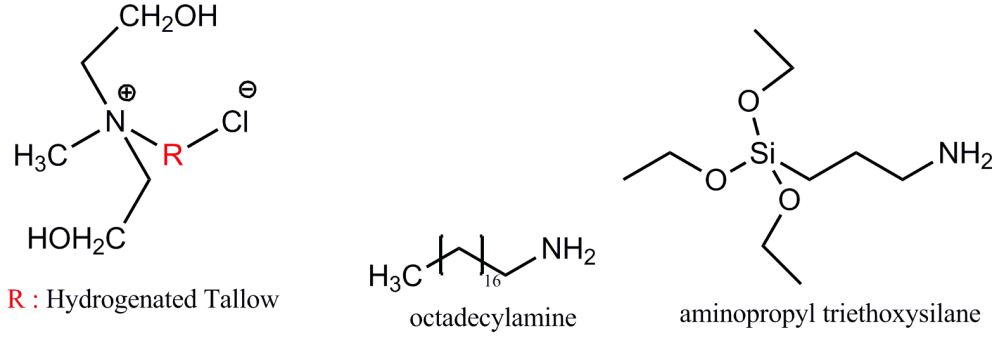

FIGURE 2 Organo-modifier groups of nanoclays [Color figure can be viewed at wileyonlinelibrary.com]

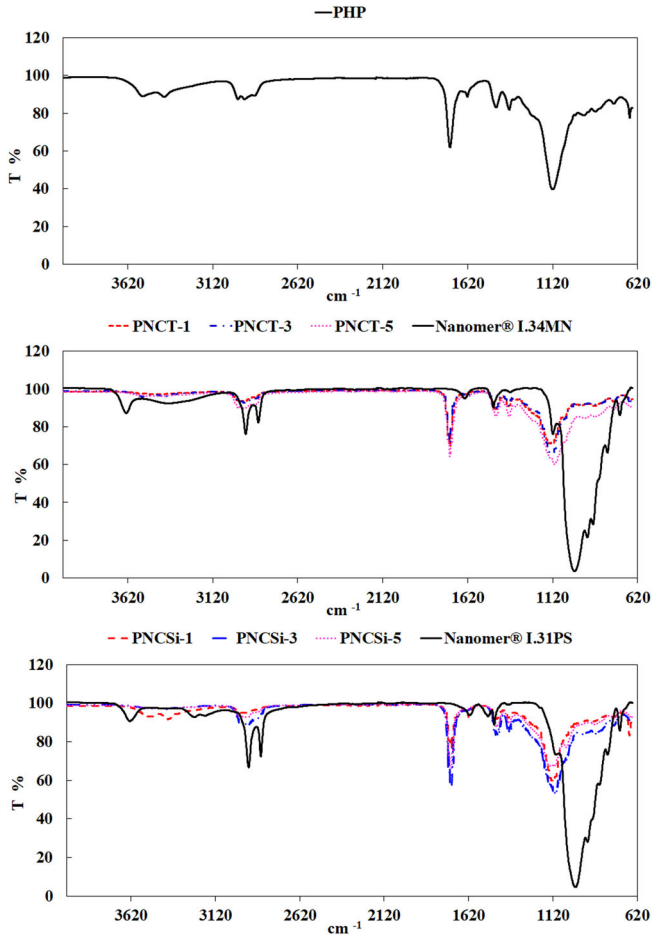

FIGURE 3 Comparative FTIR spectrums of the PHP foam (a), polyHIPE nanocomposites and the nanoclays (b) and (c). PHP, neat polyHIPE foam; polyHIPE, poly(high internal phase emulsion) [Color figure can be viewed at wileyonlinelibrary.com]

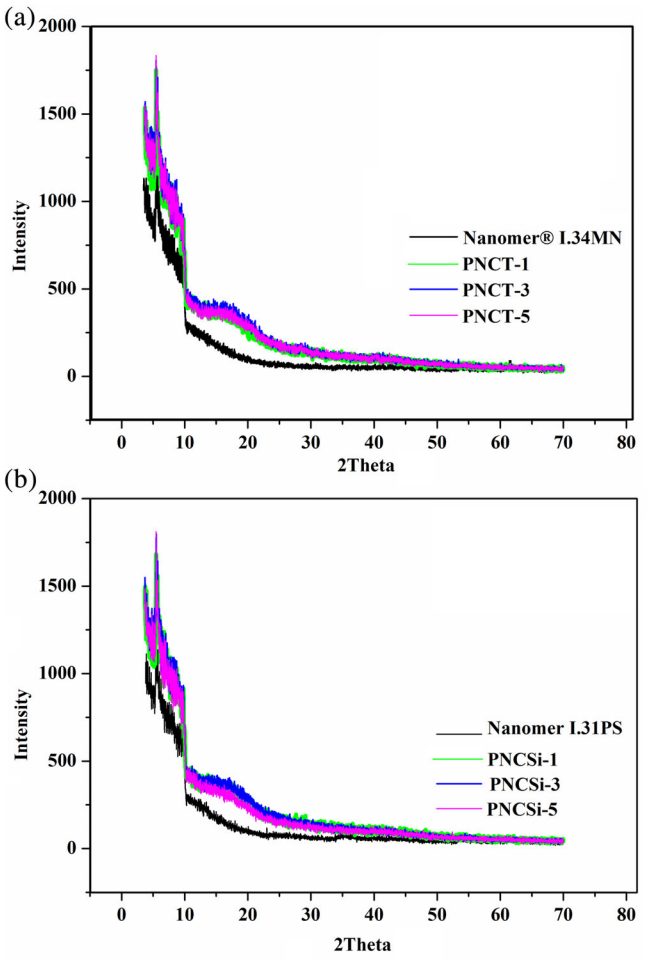

FIGURE 4 XRD patterns of the polyHIPE nanocomposites and the nanoclays. polyHIPE, poly(high internal phase emulsion); XRD, X-ray diffraction [Color figure can be viewed at wileyonlinelibrary.com]

suggested that *β*-myrcene-based polyHIPE/nanoclay composites are good candidates especially for energy storage and separation applications.

2 | EXPERIMENTAL

2.1 | Materials

β-Myrcene (technical grade, MG International Fragrance Company: Gülçiçek Kimya), EGDMA (98%, Sigma–Aldrich), Pluronic® L-121 (poly(ethylene glycol)-*block*-poly(propylene glycol)-*block*-poly(ethylene glycol), Mn, ~4400, non-ionic surfactant; Sigma–Aldrich), Nanomer® I.34MN (surface-modified MMT nanoclay, contains 25–30 wt% methyl dihydroxyethyl hydrogenated tallow ammonium; Sigma–Aldrich), Nanomer® I.31PS (surface-modified MMT nanoclay, contains 15–35 wt% octadecylamine and 0.5–5 wt % aminopropyltriethoxysilane; Sigma–Aldrich), potassium

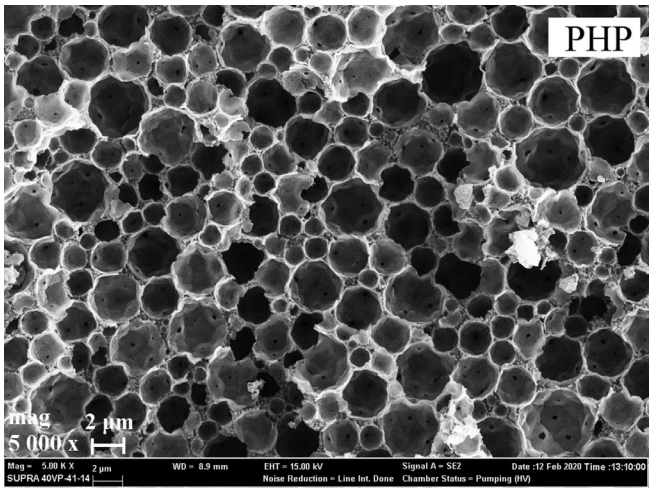

FIGURE 5 SEM image of the PHP foam. PHP, neat polyHIPE foam; SEM, scanning electron microscopy

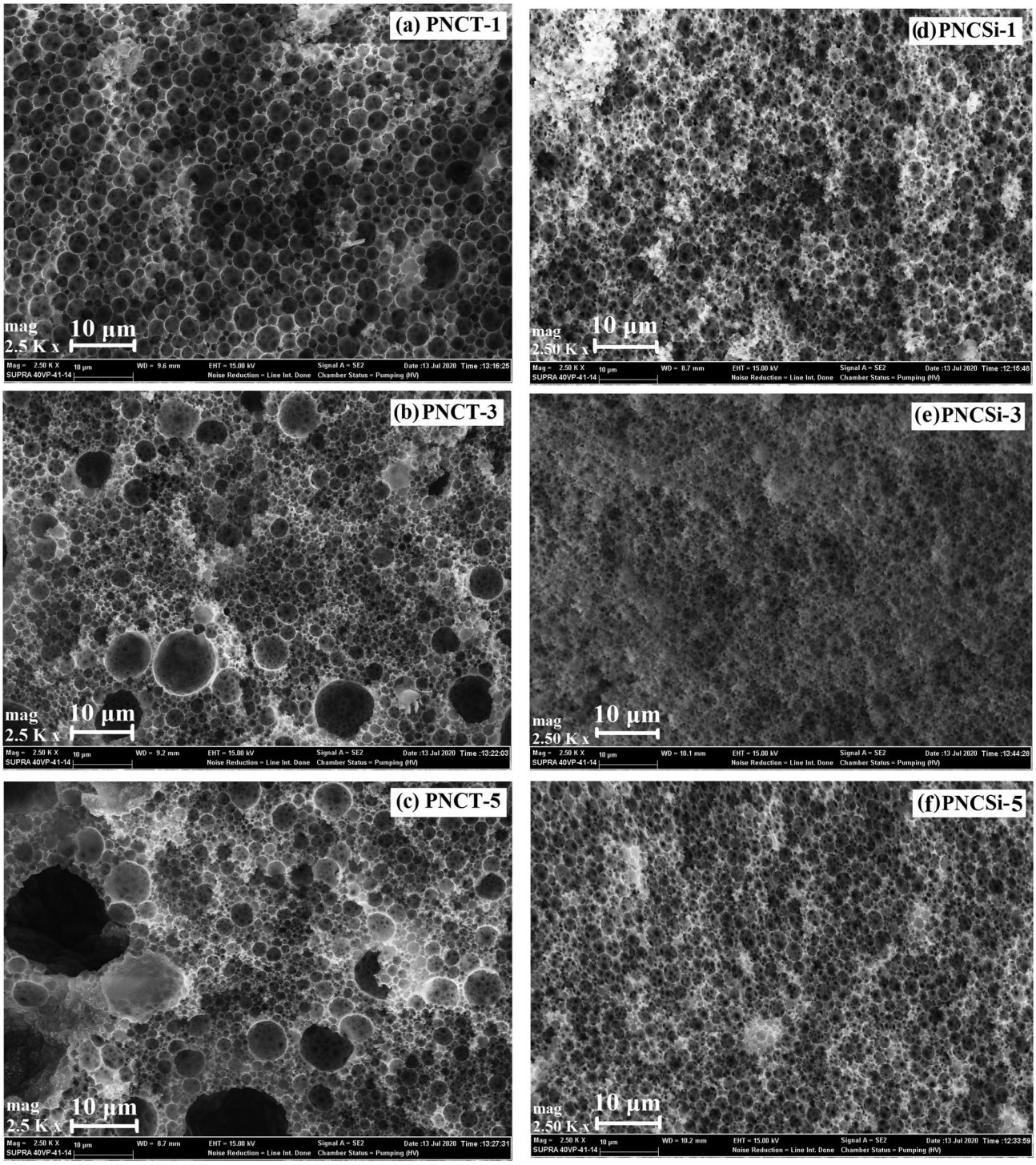

FIGURE 6 SEM images of the polyHIPE nanocomposites: (a) PNCT-1, (b) PNCT-3, (c) PNCT-5, (d) PNCSi-1, (e) PNCSi-3, and (f) PNCSi-5. SEM, scanning electron microscopy; polyHIPE, poly(high internal phase emulsion)

persulfate (KPS; ≥99.0%, ACS reagent), and calcium chloride hexahydrate ($CaCl_2.6H_2O$; 98%, Sigma–Aldrich) were used as received. In all experiments ultrapure double distilled deionized water was used. The chemical structures of the monomers and the organo-modifier groups of nanoclays are presented in Figures 1 and 2, respectively.

2.2 | Synthesis of neat polyHIPE and polyHIPE nanocomposites

In all case,s polyHIPEs were prepared with 90 vol% of nominal porosity. Synthesis of the neat polyHIPE foam (PHP) was achieved according to the previously described

TABLE 1 Morphological properties of polyHIPEs

Sample	Nanoclay (NC)	NC (wt%)	CS (μm)	IPS (μm)	δ_{BET} (m^2g^{-1})
PHP	—	—	3.21 ± 0.15	0.29 ± 0.03	14.05
PNCT-1	Nanomer® I.34MN	1	3.23 ± 0.06	0.50 ± 0.02	20.51
PNCT-3	Nanomer® I.34MN	3	2.57 ± 0.13	0.51 ± 0.03	15.71
PNCT-5	Nanomer® I.34MN	5	2.50 ± 0.07	0.62 ± 0.03	14.73
PNCSi-1	Nanomer® I.31PS	1	2.62 ± 0.06	0.55 ± 0.03	17.46
PNCSi-3	Nanomer® I.31PS	3	2.85 ± 0.06	0.59 ± 0.02	18.58
PNCSi-5	Nanomer® I.31PS	5	3.06 ± 0.04	0.60 ± 0.03	19.94

Abbreviations: CS, cavity size; IPS, interconnected pore size; PHP, neat polyHIPE foam; polyHIPE, poly(high internal phase emulsion).

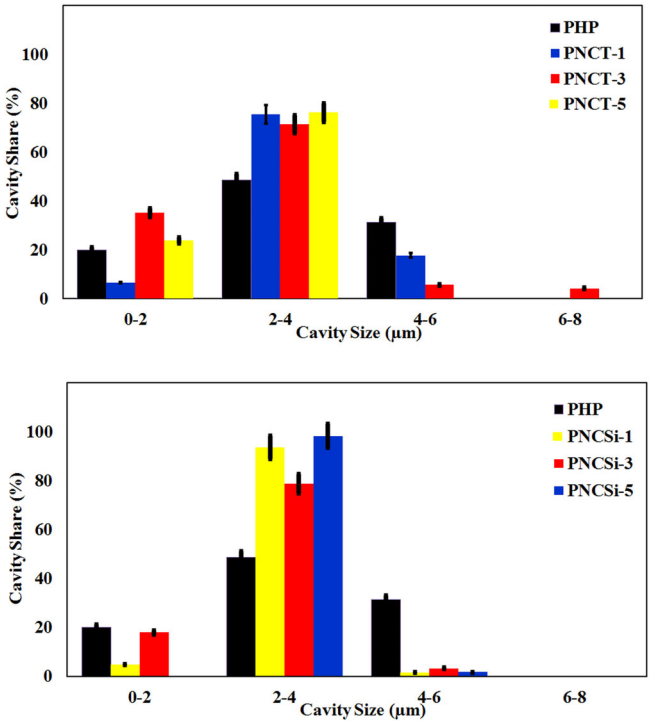

FIGURE 7 Cavity share graphs for the PHP foam and the polyHIPE nanocomposites. PHP, neat polyHIPE foam; polyHIPE, poly(high internal phase emulsion) [Color figure can be viewed at wileyonlinelibrary.com]

procedure.[30] For this purpose: 5 ml of continuous phase was prepared by mixing *β*-myrcene (5 ml, 29.1418 mmol), EGDMA (5 ml, 26.4857 mmol), Pluronic® L-121 (3 ml, 0.6859 mmol), and KPS (0.55626 mmol) in a round-bottom reactor equiped with an overhead stirrer. Afterward, 45 ml of internal phase containing 1 wt% of $CaCl_2.6H_2O$ was added dropwise with the help of a peristaltic pump under consant stirring (400 rpm) and pumping rate (50 rpm). Once addition of the internal phase was completed, stirring was continued for an extra 30 min to obtain homogeneous distribution of emulsion droplets. Thereafter, resulting water-in-oil (w/o) type HIPE was transferred into a lidded glass container and placed in an air-circulating constant temperature oven and kept at 60°C for 24 h for the completion of crosslinking. After 24 h, crosslinked PHP was removed from the glass container and then purified with ethanol in a Soxhlet apparatus for 24 h. Then dried under vacuum at 40°C until the constant weighing was available.

PolyHIPE nanocomposites were synthesized by following the given procedure above in general. The only difference between the procedures was the inclusion of nanoclay particles in the continuous phase. For this purpose either Nanomer® I.34MN or Nanomer® I.31PS was used as organo-modified nanoclay particles. PolyHIPE nanocomposites were synthesized by using 1, 3 or 5 wt% of nanolay particles. In this way six different polyHIPE nanocomposites were obtained. The polyHIPE nanocomposites, which were synthesized by the incorporation of Nanomer® I.34MN and Nanomer® I.31PS, were designated by PNCT-x and PNCSi-x, respectively. In this naming x is designating the amount of nanoclay loading.

2.3 | Characterization

In order to confirm the chemical structure of resulting polyHIPEs and demonstrate successful incorporation of nanoclay's into polyHIPE foams, FTIR analysis was performed by using Perkin Elmer Spectrum 100 FT-IR.

The nanoclay content of the PHP and polyHIPE nanocomposites (PNCT-x and PNCSi-x) were determined via gravimetrical analysis. For this purpose, all polyHIPE samples were first dried for 24 h under vacuum at 105°C. Then the following procedure was used for the calculation of residual char: ~ 0.3 g of sample was put into a porcelain crucible which was previously brought to constant weight at 900°C, and the total weight was noted. Precarbonization of the samples was performed by heating on a bunsen burner. Afterward, porcelain crucible was heated for 3 h in a muffle furnace at 650°C. In

TABLE 2 Gravimetrically calculated residual char contents, mechanical and thermal properties

Sample	Residual char (wt%)	ε_c (MPa)	σ_c(MPa)	T_{d5} (°C)	T_{d50} (°C)	T_g (°C)
PHP	1.94	17.80 ± 0.59	0.39 ± 0.03	220.3	398.6	107.7
PNCT-1	2.46	33.51 ± 1.40	16.54 ± 0.20	250.0	405.3	110.1
PNCT-3	3.78	20.01 ± 1.02	13.06 ± 0.12	241.3	401.5	111. 1
PNCT-5	4.70	18.76 ± 0.61	8.80 ± 0.15	210.7	397.2	109.1
PNCSi-1	2.03	13.72 ± 0.35	7.92 ± 0.10	206.8	399.7	111.3
PNCSi-3	3.61	15.20 ± 0.50	9.80 ± 0.13	261.6	399.9	109.8
PNCSi-5	4.94	19.81 ± 1.21	9.99 ± 0.09	269.6	401.8	107.6
Nanomer® I.34MN	74.42	—	—	—	—	
Nanomer® I.31PS	71.88	—	—	—	—	

Note: Mechanical properties, thermal stability indicators, and T_g temperatures of the resulting polyHIPEs.
Abbreviations: ε_c, compression modulus; σ_c, compressive strength; PHP, neat polyHIPE foam; polyHIPE, poly(high internal phase emulsion).

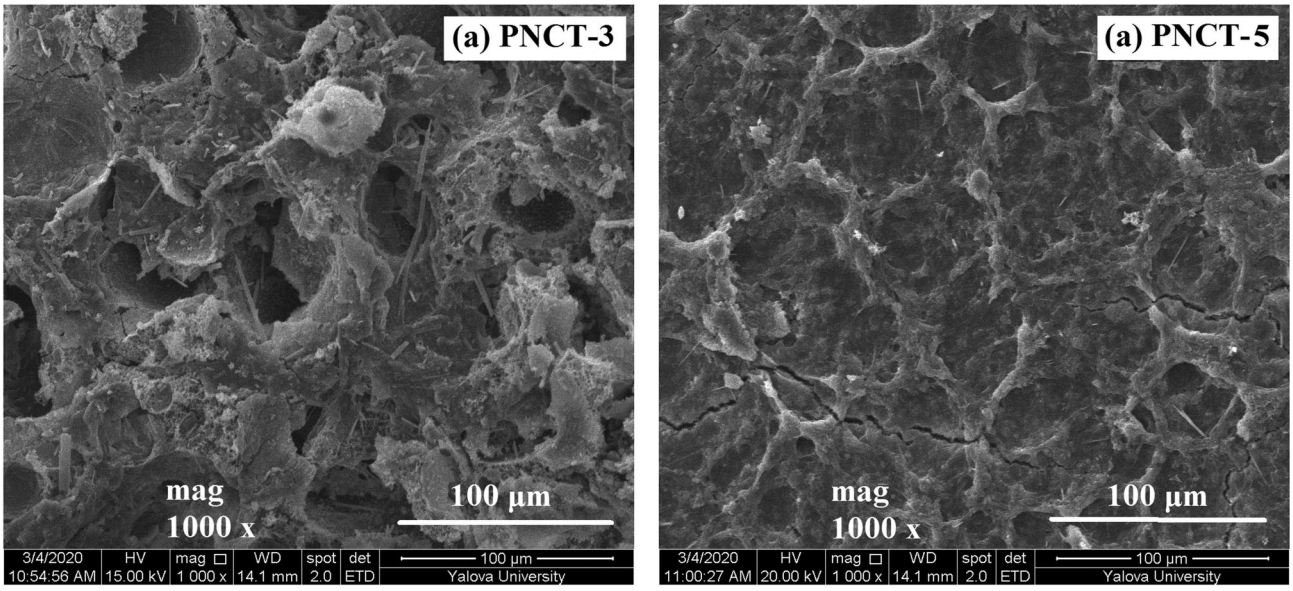

FIGURE 8 SEM micrograph of the clay agglomerates observed in the PNCT-3 and PNCT-5 nanocomposites containing (a) 3 wt% and (b) 5 wt% of the Nanomer® I.34MN

the end porcelain crucible was cooled in a dessicator to room temperature before reweighing. The final char percentage was calculated from the weight difference. Gravimetrical analysis was repeated three times for each sample. In addition to the polyHIPE samples, gravimetric analysis was also performed for the Nanomer® I.34MN and Nanomer® I.31PS nanoclays. In addition, FTIR analysis was performed on the residual chars of each sample to confirm the chemical structure.

Nanocomposite structure was confirmed by X-ray difraction (XRD) analysis. The XRD data was collected on a Bruker axs D8 Discover brand HR-XRD diffractometer. For this purpose the data was recorded in the 2θ range from 0° to 70° and counting time per step of 2 min.

Pore structure of the polyHIPEs was investigated by scanning electron microscopy (SEM; ZEISS Supra 40 VP). For this aim, polyHIPE samples were first coated with gold. For each sample average cavity size (CS) and interconnected pore size (IPS) was calculated over the taken SEM images. For the calculation of average CS, the diameter of over 100 cavities were taken, while IPS were calculated by taking over 150 measurements from the interconnected pores. Then each measurement was multiplied with a correction factor $(2/3^{1/2})$[31] before calculating the statistical average and error.

Brunauer-Emmet-Teller (BET) specific surface area (δ_{BET}) of the polyHIPEs was measured by using Micromeritics Gemini VII Surface Area and Porosity Analyzer. Before the measurement all samples were degassed on

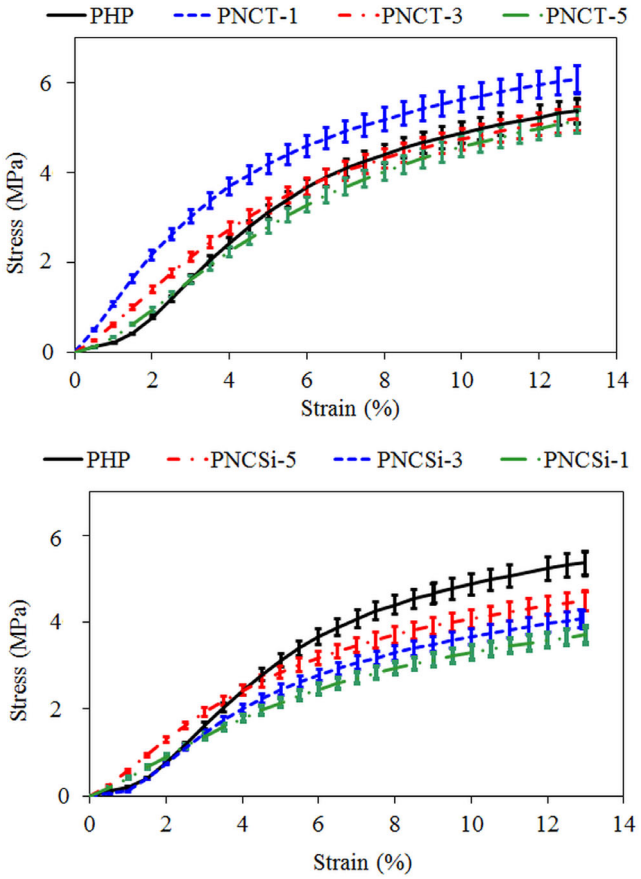

FIGURE 9 Stress–strain plots of the PHP foam and polyHIPE nanocomposites. PHP, neat polyHIPE foam; polyHIPE, poly(high internal phase emulsion) [Color figure can be viewed at wileyonlinelibrary.com]

Micromeritics FlowPrep 060 Sample Degas Unit. Degassing was conducted at room temperature for 48 h, under nitrogen flow. δ_{BET} of the polyHIPEs was calculated by applying BET equation on the recorded N_2 adsorption/desorption isotherms. For each polyHIPE sample, δ_{BET} was calculated from the arithmetic average of three different measurement conducted by using three different specimens.

Mechanical strength of the polyHIPEs was investigated in terms of compressive properties at room temperature. For this purpose five different specimens with identical dimensions (15 mm height × 10 mm width) were prepared for each polyHIPE sample. Testing specimens were not pretreated (e.g., breaking, cutting, or dividing) and used as obtained. The tests were performed by using a ZwickRoell Z020 Universal Testing Machine under 10 kN uniaxial compressive force according to ASTM D1621-04a testing standard (Standard Test Method for Compressive Properties of Rigid Cellular Plastics). The data of the measurements were recorded on the testXpert II Testing Software and representative stress/strain plots were taken from the software. The compression modulus (ε_c) of the samples was calculated from the initial slope of the stress/strain plots, while the compressive strength (σ_c) was calculated as the strength at where 13% compression was achieved.

Thermal stability of the polyHIPEs was investigated via performing thermo gravimetrical analysis (TGA). For this purpose, TGA thermograms were recorded by using Mettler Toledo TGA/DSC 3+ STAR system. TGA was conducted under N_2 flow between 30 and 650°C, and at a heating rate of 10°C/min. Glass transition temperature (T_g) of the polyHIPEs were determined under N_2 flow by using Mettler Toledo TGA/DSC 3+ STAR system. For each sample three scans (heating–cooling–heating) was carried out between −30 and 200°C at a heating rate of 10°C/min.

3 | RESULTS AND DISCUSSION

Emulsions are thermodynamically unstable complex systems mainly composed of two immiscible liquid phases (usually oil and water) and additional components, such as surfactants, initiators, and so forth. The first requirement of forming a stable emulsion is to reduce the surface tension between the two phases. At this respect, surfactants and energy input is used to disperse one of the liquid phases in the other. The time that emulsions maintain stability depends on many parameters including surfactant type and emulsion composition. The presence of nanoparticles in the emulsion composition can also negatively affect the stability due to the gravitational force. Therefore, modifying the nanoparticle surface can be used as a suitable tool for increasing the miscibility of the nanoparticles in both phases.[12,13] As similar to the conventional emulsions, HIPEs are also thermodinamically unstable and assembling nanoparticles into HIPEs might accelerate the emulsion destabilization processes, such as coalesance and sedimentation. On the other hand, polyHIPE nanocomposites obtained from HIPE templates combined with nanoparticles compatible with the emulsion phases might also have the advantages of the functionality that bring by nanoparticles. In addition, nanoclay particles can also serve as nucleating agents to obtain polyHIPEs with smaller cavities and higher densities.[32] In this respect, polyHIPE nanocomposites were synthesized by incorporating two different types of organo-modified MMT nanoclay into the continuous phase of β-myrcene and EGDMA-based HIPE templates. Since polyHIPE properties are the reflections of precursor HIPEs,[6] nanoclay selection was performed by considering the emulsion stability, and as well as the functionality of the resulting nanocomposites. In this respect, selected nanoclays have

oil compatible surface groups that are promoting to sustain emulsion stability. The influences of organo-modified nanoclay type and the amount of nanoclay loading were investigated in terms of morphological, mechanical, and thermal properties. With this aim, properties of the resulting polyHIPE/nanoclay composites were compared with the properties of the PHP.

Chemical structures of the obtained polyHIPEs were confirmed via FTIR analysis. Comparative FTIR spectrums of the PHP foam, polyHIPE nanocomposites and nanoclays are all presented in Figure 3. In Figure 3(a) the broad absorption peaks appeared at 2970, 2931, and 2870 cm^{-1} at the spectrum of the PHP foam can be assigned to the —CH_3, —CH_2, and —CH asymmetric stretching vibrations, respectively. In addition, the absorption peaks around 1444 and 1376 cm^{-1} can be attributed to the characteristic —CH_2 and —CH_3 bending vibrations, while the absorption peak arise at ~1724 cm^{-1} can be ascribed to the ester type C═O stretching. The significant absorption peak at around 990 cm^{-1} can be ascribed to the sp^2 C—H bending vibrations. The small signal appeared at ~735 cm^{-1} can be explained as the —CH_2 rocking vibration, and the lower intensity of this absorption peak can be attributed to the restricted rocking movement in the polymer chains.[33] In addition to all, the peaks arised at around 3601 cm^{-1} can be ascribed to the —OH stretching.

In the studies of clay minerals, stretching and bending vibrations of the structural —OH and Si—O groups of nanoclay plays a decisive role in the identification of MMT and different kinds of modified MMT. In this context, it can be clearly seen from Figure 3(b) and (c) that both Nanomer® I.34MN and Nanomer® I.31PS have exhibited similar FTIR spectrums. The obvious absorption bands appeared at ~3620 cm^{-1} can be attributed to the —OH stretching vibrations of the MMT. For the surface-modified nanoclays the intensity, frequency, and band shape of the absorption peaks can be changed due to the type and concentration of organo-modifier groups. Consequently, some characteristic peaks might be shifted. It can be seen from the spectrums of both nanoclays that the complex streching band of Si—O, which is usually appeared at around 1030 cm^{-1}, and the shoulder bands were also shifted to ~990 cm^{-1} and to ~916 cm^{-1}.[34] The bands appeared at ~916 cm^{-1} can be ascribed to the AlAlOH bending vibrations of MMT. In addition, the small shoulder peaks observed at ~882 cm^{-1} in the spectrum of Nanomer® I.34MN (Figure 3(b)), and ~ 842 cm^{-1} in the spectrum of Nanomer® I.31PS (Figure 3(c)) can be attributed to the AlMgOH bending vibrations of MMT.[35] The absorption bands that arised at ~2920 and at ~2850 cm^{-1} can be ascribed to C—H stretching of the CH_3 and CH_2 groups, respectively. Finally, the peak observed at ~1470 cm^{-1} can be explained as the bending modes of the vibration of CH_2 groups.[36] On the other hand, the absorption band apperared at ~3242 cm^{-1} in the spectrum of Nanomer® I.31PS (Figure 3(c)) can be ascribed to the —NH stretching band of the organo-modifier group. When compared the spectrums of the resulting PNCT-x and PNCSi-x nanocomposites (presented in Figure 3(b),(c), respectively) with the spectrums of the PHP foam (Figure 3(a)) and the nanoclays, the characteristic absorption peaks appeared due to the nanoclays and polymer chains confirms the successful incorporation of nanoclay particles in polyHIPE matrix. In this respect, from the spectrum of PNCT-x and PNCSi-x nanocomposites (Figure 3(b) and (c), respectively) the complex absorption band arise at ~1119 cm^{-1} can be explained with the overlap of the sp^2 C—H bending vibrations of the polymer chains with the Si—O stretching vibrations of nanoclay's. The peaks observed at ~2960, 2936, and 2850 cm^{-1} can be ascribed to the —CH_3, —CH_2, and —CH asymmetric stretching vibrations, respectively. It can be seen from Figure 3(b),(c) that the shape of these absorption bands was slightly changed in the PNCT-x and PNCSi-x nanocomposites, as compared to the PHP foam (Figure 3(a)) and the nanoclay particles (Figure 3(b),(c)). It can be seen from the spectrum of PNCSi-1 nanocomposite given in Figure 3(c) that this nanocomposite has characteristic signal of —NH_2 groups appeared at ~3514 cm^{-1}. However, as the amount of nanoclay increased, this peak observed as an overlapping broad band in the same region, for the PNCSi-3 and PNCSi-5 nanocomposites (Figure 3(c)) due to the reduce of its intensity.

The dispersion of nanoclay particles in polymer matrix was investigated through XRD. By detecting the shifted diffraction peaks, the change of interlayer spacing or gallery of the nanoclay was evaluated. The XRD patterns of Nanomer® I.34MN, Nanomer® I.31PS and polyHIPE nanocomposites are presented in Figure 4. In addition, the degree of dispersion was determined by calculating d-spacing (d001) through Bragg's Law. In Figure 4(a) the basic, secondary, and the tertiary peaks of Nanomer® I.34MN were detected at 2θ values of 5.41° (d001 = 1.63 nm), 3.55° (d001 = 2.49 nm), and 61.66°, respectively. The peak patterns of the PNCT-x nanocomposites (Figure 4(a)) were found to be in accordance with Nanomer® I.34MN and the basic peaks of the nanoclay were also observed in PNCT-x samples. However, in the XRD patterns of PNCT-1, PNCT-3, and PNCT-5, the primary peak of the nanoclay was observed to arise at 2θ values of 5.56° (d001 = 1.59 nm), 5.70° (d001 = 1.55 nm), and 5.84° (d001 = 1.51 nm), respectively. In addition, the secondary peak of the nanoclay was found to be shifted to 2θ values of 3.71°

(d001 = 2.38 nm), 3.74° (d001 = 2.36 nm), and 3.75° (d001 = 2.36 nm) in the PNCT-1, PNCT-3, and PNCT-5 nanocomposites, respectively. In addition, it was observed that with the increase in the amount of nanoclay in the polymer matrix the peaks get narrower and their intensity was increased. The reason of this increase might be explained by better crystallinity values. However, the shifting of the two basal peaks of the nanoclay to higher angles in PNCT-x nanocomposites and the decrease of the d-spacing, point to a low dispersion of nanoclay particles in the polymer matrix. In Figure 4(b), the peak patterns of Nanomer® I.31PS were observed at 2θ values of 5.42° (d001 = 1.63 nm) and 3.92° (d001 = 2.25 nm) as a basic and a secondary peak, respectively. Besides, two small and broader peak patterns were also detected at the 2θ values of 35.30 and 61.70°. These peaks are the characteristic peak trends of the nanoclay. By the incorporation of 1 wt% of nanoclay, the 2θ value of the secondary peak was shifted to 3.81° corresponding to a d-spacing of 2.32 nm. The increased d-spacing in the PNCSi-1 nanocomposite can be explained by the increased distance between the clay galleries. However, with the increase of nanoclay loading this peak was shifted slightly to higher angles and arised at 2θ values of 3.95° (d001 = 2.24 nm), and 4.09° (d001 = 2.16 nm) for the PNCSi-3 and PNCSi-5 samples, respectively (Figure 4(b)). This result shows that increasing the amount of nanoclay loading tends to decrease the distance between nanoclay galleries. In addition to all, it was observed that the peaks that were reflected in the patterns of the nanoclay at the 2θ values of 35.30 and 61.70° were not reflected in the XRD patterns of PNCSi-x nanocomposites (Figure 4 (b)). The absence of these two characteristic peaks of the nanoclay might be explained by the exfoliation of nanoclay with the interlayer distance over the value of 2.2 nm.[36–38]

Pore structure of the obtained polyHIPEs were observed by using SEM, and displayed in Figures 5 and 6. According to the SEM image in Figure 5 the PHP foam is composed of almost spherical cavities and interconnected pores. However, sparse and small size interconnections are indicating a monolithic structure with low permeability. The average CS and IPS of the polyHIPEs are presented in Table 1. According to Table 1, the average size of the cavities and interconnected pores of the PHP foam were calculated as 3.21 and 0.29 μm, respectively.

The SEM images in Figure 6 is presenting the open-porous structure of the polyHIPE nanocomposites. According to Table 1, average size of the cavities of the polyHIPE nanocomposites were altered between 2.57 and 3.23 μm, while interconnected pore sizes were changed between 0.50 and 0.62 μm. Accordingly, it can be safely stated that addition of nanoclay particles significantly improved the morphological structure and increased the openness of the foams by leading to the formation of more and larger interconnected pores. When the morphological properties of the PNCT-1, PNCT-3, and PNCT-5 nanocomposites prepared by using Nanomer® I.34MN were evaluated, CSs were found to be decreased from 3.23 to 2.50 μm with the increasing amount of nanoclay. On the other hand, IPS were found to be increased from 0.50 to 0.62 μm at the same conditions. It has been observed that the use of Nanomer® I.31PS for the preparation of polyHIPE nanocomposites results in smaller cavities and the formation of larger interconnected pores compared to the PHP foam. In these nanocomposites (PNCSi-1, PNCSi-3, and PNCSi-5), the average CS was found to be changed between 2.62 and 3.06 μm, while the size of interconnected pores were altered between 0.55 and 0.60 μm. In addition, according to the cavity share graphs presented in Figure 7, these nanocomposites have narrower CS distribution compared to their counterparts synthesized using Nanomer® I.34MN. These results are indicating that the organo-modifier groups of the nanoclay particles and the amount of nanoclay loading have strong role on the average CS and CS distribution.

It is known from the previous studies that using nanoparticles with compatible surface groups provide benefit for obtaining stable emulsions. Compatible surface groups assist decreasing the surface tension between the oil and water phases of the emulsions and leads homogenous dispersion of nanoparticles within the oil phase. In addition, surface modifier groups also support dispersing high amount of internal phase within the oil phase. Since the average cavity size is determined by the emulsion droplets, it is also dependent on the emulsion stability instead of other experimental parameters (i.e., surfactant amount, crosslinker amount, agitation rate, and so forth).[6] In general, the decrease in average cavity sizes can be explained by the increased emulsion stability due to nanoclay loading. It can be concluded that the presence of organo-modifying groups on the nanoclay surface supports the stabilization process. This situation is basically relied on the change of total polarity and viscosity of the oil phase. Variation of the average CS at different nanoclay loadings might be attributed to the decrease of the viscosity ratio of internal phase to disperse phase. This result is consistent with the findings of previous studies.[20,21,23,25,31,39–41]

Due to the presence of surface modifier groups, it was expected that nanoclay particles distributed in the continuous phase were embedded within the cavity walls of the resulting polyHIPE nanocomposites. Accordingly, embedded particles was also expected not to swept away during the purification step. In order to support this

phenomenon, gravimetrical analysis was conducted for the determination of final nanoclay content of each polyHIPE nanocomposite. Since the residual char content is the remaining inorganic content after carbonization, it is showing the amount of nanoclay loading of polyHIPE nanocomposites. To make a better assessment, the same experimental approach was also used for the calculation of residual char content of the PHP, Nanomer® I.34MN and Nanomer® I.31PS. After gravimetrical analysis FTIR was used for the determination of the chemical structures of residual chars. The residual char contents are presented in Table 2 and comparative FTIR spectrums are presented in Supplementary Information (SI) file (Figures S1 and S2). According to Table 2, it was concluded that the residual char content of the polyHIPE nanocomposites were in accordance with the amounts of the added nanoclay particles. The slight difference between the amount of nanoclay loading and residual char content might be attributed to the removal of the water present in the clay galleries.[21,42,43] In addition to the residual char content, comparison of the FTIR spectrums of residual chars presented in SI file (Figures S1 and S2) and SEM–EDX results presented in Figures S3 and S4 is also confirming the successful nanoclay loading.

The influence of nanoclay loading on the change of BET specific surface area (δ_{BET}) was also investigated. While the BET specific surface area of the PHP foam was 14.05 m^2g^{-1}, PNCT-1, PNCT-3, and PNCT-5 nanocomposites were found to have specific surface areas of 20.51, 15.71, and 14.73 m^2g^{-1}, respectively. In addition, only a slight increase was observed for the specific surface areas of the PNCSi-1, PNCSi-3, and PNCSi-5 nanocomposites. As a result of the surface area analysis, it was found that the specific surface area of these nanocomposites was 17.46, 18.58, and 19.94 m^2g^{-1}, respectively. The variation of the specific surface area of the PNCT-x nanocomposites with the increasing amount of Nanomer® I.34MN might be attributed to the variation of cavity size distribution of these foams. It can be seen from Figures 6(a) and 7 that the cavity size distribution was widened with the increasing amount of Nanomer® I.34MN. As well as the average cavity size of PNCT-3 and PNCT-5 nanocomposites decreased as compared to PNCT-1, the expansion in the cavity size distribution might also indicative of inhomogeneous distribution of nanolcay particles. The interaction between nanoclay particles is usually increased at higher loading of particles. Accordingly, clay layers tend to form large agglomerates that are less able to exfoliate as compared to the small nanoclay particles.[44] The agglomerates at higher nanoclay concentrations of Nanomer® I.34MN can be seen from the SEM images of PNCT-3 and PNCT-5 nanocomposites presented in Figure 8. This situation might be eventually attribute to the effect of the surface groups of the nanoclays (Figure 2). Since Nanomer® I.34MN has only methyl dihydroxyethyl hydrogenated tallow ammonium group and Nanomer® I.31PS has both octadecylamine and aminopropyltriethoxysilane groups it is more compatible with relatively polar continuous phase of the HIPEs.

The relation between the mechanical properties of polyHIPE nanocomposites and nanoclay type and loading were studied in terms of compressive properties. The representative stress versus strain plots of the PHP foam and nanoclay filled polyHIPE nanocomposites recorded according to the dependence on the nanoclay type and loading are shown in Figure 9, while corresponding compression modules are presented in Table 2. According to Table 2, the PHP foam has a compression modulus of 17.80 MPa. In addition, concerning the compressive properties, significant differences were observed depending on the nanoclay type. In between two organo-modified nanoclay, Nanomer® I.34MN contributed to the improvement of mechanical properties, significantly while Nanomer® I.31PS was found to have less effect. In particular, Nanomer® I.34MN filled PNCT-1 nanocomposite yielded highest compression modulus, corresponding to ca. 33% increment in compression modulus as compared to the PHP foam. This result shows that the hydrogenated tallow groups of the organo-modified nanoclay contributed with a noticable flexibility to polyHIPE matrice under compressive load. Although the Nanomer® I.34MN filled polyHIPE/nanoclay nanocomposites were all capable of improving the compressive strength as compared to non-filled PHP foam, a considerable decrement was observed in compression modulus depending on the increasing amount of nanoclay loading. To be more certain, 40 and 44% decrement was observed in the compression modulus of PNCT-3 and PNCT-5 nanocomposites as compared to PNCT-1, respectively. This result might be attributed to the formation of larger clay agglomerates at higher concentrations due to the strong covalent bonding between clay sheets.[44,45] According to the previous studies stress formation can be risen by agglomeration and weakened the intercalation phenomena that support the improvement of mechanical properties.[45–47] The formation of clay agglomerates by filling the polyHIPE matrix with 3 and 5 wt% of Nanomer® I.34MN can also be seen from the SEM images presented in Figure 8.

According to Table 2, the addition of 1 wt% of Nanomer® I.31PS into the precursor HIPE template, decreased the compresion modulus ca 23%, as compared to PHP foam. This result was shown that at lower concentrations Nanomer® I.34MN provided better distribution in the polyHIPE matrix then Nanomer® I.31PS. However, it has also been found that the polyHIPE matrix was slightly strengthened with increasing

Nanomer® I.31PS concentration. The compression modulus increased by about 11% of the compression modulus of the PHP foam when the nanoclay loading was 5% by weight. This situation is also indicating that at higher concentrations Nanomer® I.31PS was distributed more homogenously as compared to corresponding concentrations of Nanomer® I.34MN. Accordingly, the transfer of stress from nanoclay to polymer matrix was found to be effectively increased. In addition to all, it was also observed that the variation of the compressive strength was always proportional with the change of compression modulus, for each polyHIPE sample (Table 2).

As compared with the previously published results, the contribution of the β-myrcene units on the mechanical properties of nanoparticle incorporated polyHIPEs is very distinctive. For instance, Moghbeli and Shahabi[48] reported polystyrene based elastomeric poly(HIPE) nanocomposite foams that were synthesized by using 2-EHA and DVB as crosslinker comonomers and organo-modified nanoclay particles as reinforcing agent. According to their findings, the highest observed value for the compression modulus of polyHIPE foams containing nanoclay was reported as 5.14 MPa. Comparison of the mechanical properties of the obtained polyHIPE nanocomposites with our previous results also clearly shows that replacing styrene with β-myrcene significantly improves the compression properties.[20] According to our previously published results, while bare poly(styrene-*co*-DVB) foams have compression modulus of 7.17 MPa, addition of a 3 wt% nanoclay having a reactive intercalant group revealed compression moduli of 12.16 MPa.[20] Compared to our study, the compression modulus of the neat poly(β-myrcene-*co*-EGDMA) foam (PHP), which are specified as 17.80 MPa, is even higher than poly(styrene-*co*-DVB) foams containing 3 wt% of nanoclay. On the other hand, β-myrcene based polyHIPE/nanoclay foams also exhibited higher compression modulus and strength as compared to polyester/nanoclay foams synthesized by the crosslinking of organo-modified nanoclay incorporated unsaturated polyester and divinylbenzene based HIPE templates.[21] As a result of our study, it can be safely concluded that using β-myrcene and EGDMA based HIPE templates for polyHIPE foam preparation has a great influence on the improvement of mechanical properties due to the reduced brittleness of the resulting polymer network.

The influence of nanoclay loading on the thermal stability of resulting polyHIPE nanocomposites was investigated by means of TGA. The TGA and DTG thermograms are presented in Figure 10, while thermal stability indicators determined from the thermograms are presented in Table 2. In Table 2, T_{d5} and T_{d50} are representing the onset and midpoint degradation temperatures that are corresponding to the temperatures at which 5 and 50 wt% of weight loss occurred, respectively. According to the TGA thermograms presented in Figure 10 while PHP foam exhibited two stage decomposition, PNCT-x and PNCSi-x nanocomposites exhibited three stage continuous decomposition. For all samples the first slight mass loss observed up to ~105°C can be explained by the removal of trapped water molecules in between the cavities. The second mass loss observed from the thermograms of PNCT-x and PNCSi-x nanocomposites can be explained by decomposition of the surface groups of nanoclay particles. On the other hand, the massive mass loss that was observed between ~360 and ~470°C for all samples can be attributed to decomposition of polymer chains.

Thermal indicator temperatures presented in Table 2 demonstrated that incorporating nanoclay particles significantly influence the onset and midpoint degradation temperatures. In terms of PNCT-x nanocomposites, adding 1 wt % of Nanomer® I.34MN was found to increase the T_{d5} temperature as 30°C. However, T_{d5} was found to decrease significantly with the increasing concentration of nanoclay. This result might be attributed to non-homogenous distribution of nanoclay particles and it is consistent with the variation of morphological and mechanical properties of PNCT-x nanocomposites with nanoclay concentration. On the contrary of PNCT-x nanocomposites, while compared to the PHP foam the T_{d5} temperature of PNCSi-x nanocomposites was found to decreased about 14°C by adding 1 wt% of Nanomer® I.31PS. However with the addition of 5 wt% Nanomer® I.31PS, T_{d5} was found to increase up to 269°C. Unlike the T_{d5} temperature, the T_{d50} temperature was found to change slightly with the variation of nanoclay concentration for all samples. However PNCT-1 nanocomposite which was prepared by the addition of 1 wt% Nanomer® I.34MN was found to exhibit the highest T_{d50} temperature as compared to the PHP foam and as well as the other nanocomposites.

The DSC thermograms of the PHP foam and polyHIPE nanocomposites are presented in Figure S5 and Tg temperatures are shown in Table 2. For all samples, the inflection appeared in the heating path of the scan was attributed to T_g temperature (Figure S5). In addition, no appearance of a peak in the cooling step was attributed to the amorphous structure of the PHP foam and the nanocomposites. It can be seen from Table 2 that nanoclay incorporation led a slight change in T_g for all polyHIPE nanocomposites, as compared to the PHP foam. In addition, the slight shifting of the onset temperatures of the polyHIPE nanocomposites to higher temperatures can be

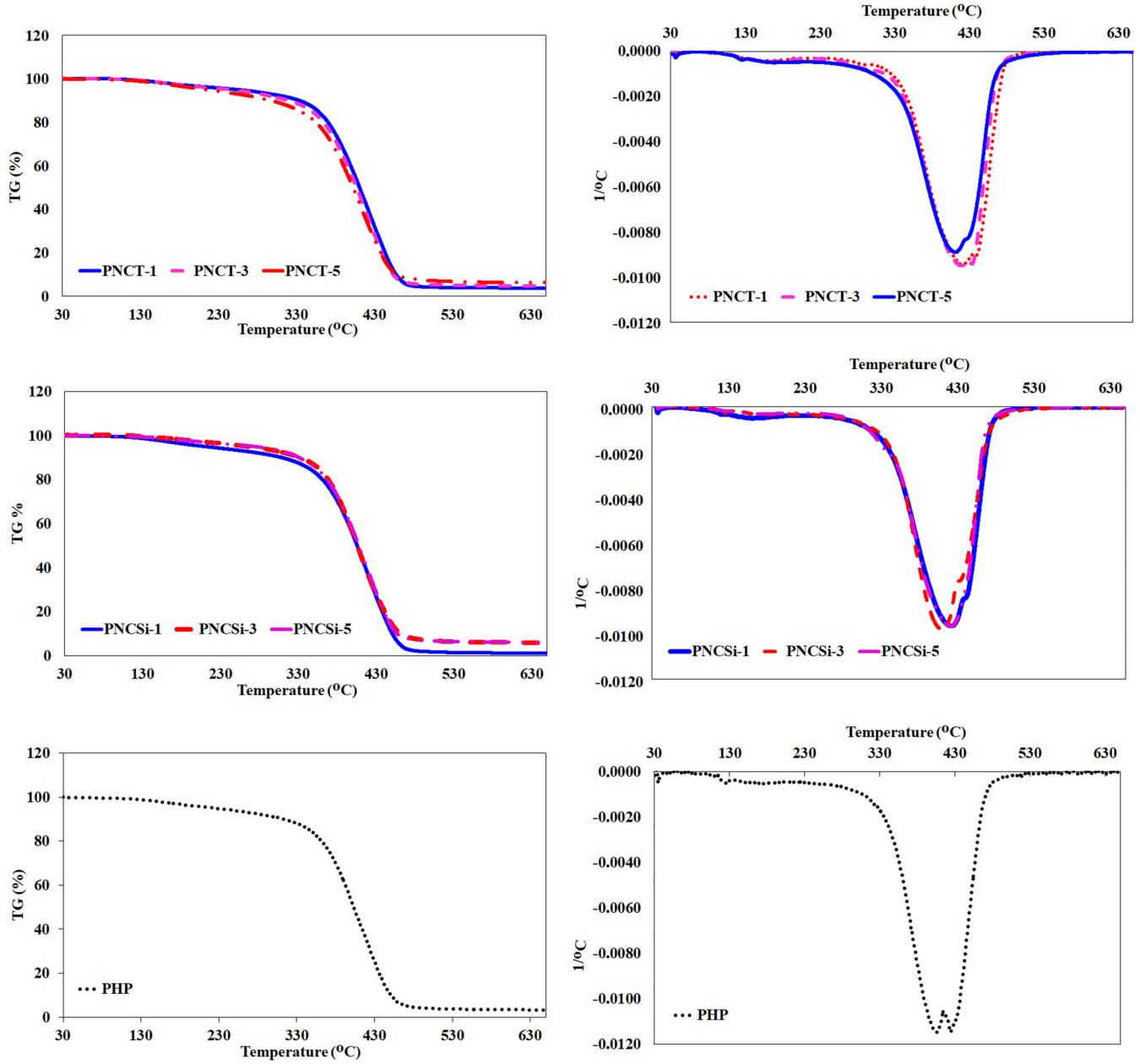

FIGURE 10 TGA and DTG thermograms of the PHP foam and the polyHIPE nanocomposites. PHP, polyHIPE foam; polyHIPE, poly(high internal phase emulsion)s; TGA, thermogravimetric analysis [Color figure can be viewed at wileyonlinelibrary.com]

explained by the decreased chain flexibility due to addition of nanoparticles.

4 | CONCLUSION

Macroporous nanocomposites were synthesized by incorporating two different organo-modified nanoclay into *β*-myrcene-based HIPEs. The improved morphological, mechanical and thermal properties of the obtained nanocomposites were demonstrated by comparing with a neat polyHIPE foam. It was shown that organo-modifier groups of the nanoclay have a great importance in terms of altering the properties. Regarding the pore morphology, addition of Nanomer® I.34MN and Nanomer® I.31PS have both improved the openness of the nanocomposite foams, as compared to neat polyHIPE foam. It was found that while the average cavity size of the obtained nanocomposites decreased, the interconnected pore sizes increased. PolyHIPE/nanoclay nanocomposite, which contains 1% Nanomer® I.34MN by weight, has the highest compression modulus and strength. In addition, it showed higher thermal stability. However, it was found that Nanomer® I31PS filled nanocomposites prepared using less than 5% by weight of nanoclay had a significant decrease in the compression properties as compared to the

unfilled polyHIPE. On the other hand, thermal stability of the Nanomer® I31PS filled nanocomposites was found to increase with the increase of nanoclay concentration. Consequently, it was found that both the organo-modifier surface groups and the concentration of the nanoclay particles have a remarkable influence on the ultimate morphological, mechanical and thermal properties of β-myrcene-based polyHIPE/nanoclay nanocomposites.

ACKNOWLEDGMENTS

Authors thanks to the MG International Fragrance Company: Gülçiçek Kimya (Gebze, Kocaeli, Turkey) for their kind donation of β-myrcene. Authors thank to the Photonics Research Center of the Gazi University for performing the XRD analysis.

ORCID

Burcu Kekevi https://orcid.org/0000-0002-2364-1957
Emine Hilal Mert https://orcid.org/0000-0003-4267-7469

REFERENCES

[1] I. Pulko, P. Krajnc, *Macromol. Rapid Commun.* **2012**, *33*, 1731.
[2] M. S. Silverstein, *Polymer* **2014**, *55*, 304.
[3] T. Zhang, R. A. Sanguramath, S. Israel, M. S. Silverstein, *Macromolecules* **2019**, *52*, 5445.
[4] N. R. Cameron, *Polymer* **2005**, *46*, 1439.
[5] M. S. Silverstein, *Prog. Polym. Sci.* **2014**, *39*, 199.
[6] H. H. Mert, M. S. Mert, E. H. Mert, *Mater. Res. Express* **2019**, *6*, 115306.
[7] A. Koler, I. Pulko, P. Krajnc, *Acta Chim. Slov.* **2020**, *67*, 349.
[8] K. Haibach, A. Menner, R. Powell, A. Bismarck, *Polymer* **2006**, *47*, 4513.
[9] A. Menner, K. Haibach, R. Powell, A. Bismarck, *Polymer* **2006**, *47*, 7628.
[10] E. Yüce, F. N. Parın, P. Krajnc, H. H. Mert, E. H. Mert, *React. Func. Polym.* **2018**, *130*, 8.
[11] E. Yüce, P. Krajnc, H. H. Mert, E. H. Mert, *J. Appl. Polym. Sci.* **2019**, *136*, 46913.
[12] A. Vílchez, C. Rodríguez-Abreu, J. Esquena, A. Menner, A. Bismarck, *Langmuir* **2011**, *27*, 13342.
[13] E. H. Mert, H. Yıldırım, A. T. Üzümcü, H. Kavas, *React. Funct. Polym.* **2013**, *73*, 175.
[14] S. Huš, P. Krajnc, *Polymer* **2014**, *55*, 4420.
[15] E. H. Mert, C. Slugovc, P. Krajnc, *eXPRESS Polym. Lett.* **2015**, *9*, 344.
[16] S. Kovčič, K. Jeřábek, P. Krajnc, C. Slugovc, *Polym. Chem.* **2012**, *3*, 325.
[17] M. R. Moghbeli, A. Khajeh, M. Alikhani, *Chem. Eng. J.* **2017**, *309*, 552.
[18] H. H. Mert, M. R. Moghbeli, S. Sajad, E. H. Mert, *React. Func. Polym.* **2020**, *151*, 104572.
[19] Z. Abbasian, M. R. Moghbeli, *J. Appl. Polym. Sci.* **2011**, *119*, 3728.
[20] F. Çira, E. Berber, S. Şen, E. H. Mert, *J. Appl. Polym. Sci.* **2015**, *132*, 41333.
[21] E. Berber, F. Çira, E. H. Mert, *Polym. Compos.* **2016**, *37*, 1531.
[22] H. H. Mert, S. Şen, *e-Polymers* **2016**, *16*, 419.
[23] E. Yüce, E. H. Mert, P. Krajnc, F. N. Parın, N. San, D. Kaya, H. Yıldırım, *Macromol. Mater. Eng.* **2017**, *302*, 1700091.
[24] E. Yüce, E. H. Mert, S. Şen, S. Saygı, N. San, *J. Appl. Polym. Sci.* **2017**, *134*, 45522.
[25] H. H. Mert, E. Tekay, N. Nugay, T. Nugay, S. Şen, *Polym. Eng. Sci.* **2018**, *58*, 1229.
[26] W. Bian, X. Lu, X. Wang, W. Xu, M. Zheng, X. Jiang, *Appl. Clay Sci.* **2020**, *190*, 105591.
[27] H. H. Mert, *Int. J. Energy Res.* **2020**, *44*, 6583.
[28] A. Behr, L. Johnen, *Chem. Sus. Chem.* **2009**, *2*, 1072.
[29] N. Bauer, J. Brunke, G. Kali, *ACS Sustain. Chem. Eng.* **2017**, *5*, 10084.
[30] E. H. Mert, B. Kekevi, *Colloid Polym. Sci.* **2020**, *298*, 1423.
[31] A. Barbetta, N. R. Cameron, *Macromolecules* **2004**, *37*, 3188.
[32] M. S. Ahmed, Y. H. Lee, C. B. Park, N. Atalla, *Asia-Pac. J. Chem. Eng.* **2009**, *4*, 120.
[33] P. Sarkara, A. K. Bhowmick, *RSC Adv.* **2014**, *4*, 61343.
[34] N. Banik, S. A. Jahan, S. Mostofa, H. Kabir, N. Sharmin, M. Rahman, S. Ahmed, *Bangladesh J. Sci. Ind. Res.* **2015**, *50*, 65.
[35] Z. Danková, A. Mockovčiaková, S. Dolinska, *Desalin. Water Treat.* **2014**, *52*, 5462.
[36] V. Mucci, J. Pérez, C. I. Vallo, *Polym. Int.* **2011**, *60*, 247.
[37] S. Ray, S. Y. Quek, A. Easteal, X. D. Chen, *Int. J. Food Eng.* **2006**, *2*, Art. 5.
[38] M. H. M. Yazik, M. T. H. Sultan, A. U. M. Shah, M. Jawaid, N. Mazlan, *Polym. Bull.* **2020**, *77*, 5913.
[39] Y. H. Lee, C. B. Park, K. H. Wang, M. H. Lee, *J. Cell. Plast.* **2005**, *41*, 487.
[40] W. Zheng, Y. H. Lee, C. B. Park, *J. Cell. Plast* **2006**, *42*, 271.
[41] Y. H. Lee, K. H. Wang, C. B. Park, M. Sain, *J. Appl. Polym. Sci.* **2007**, *103*, 2129.
[42] M. Pansu, J. Gautheyrou, *Handbook of Soil Analyses*, Springer, Berlin, Heidelberg **2006**; Chapter 1, p. 3.
[43] K. Song, G. Sandi, *Clays Clay Miner.* **2001**, *49*, 119.
[44] J. A. C. Discacciati, R. L. Oréfice, *J. Mater. Sci.* **2007**, *42*, 3883.
[45] A. K. Nikolaidis, E. A. Koulaouzidou, C. Gogos, D. S. Achilias, *Polymers* **2019**, *11*, 730.
[46] M. Atai, A. Pahlavan, N. Moin, *Dent. Mater.* **2012**, *28*, 133.
[47] S. T. Bee, A. Hassan, C. T. Ratnam, T. T. Tee, L. T. Sin, D. Hui, *Compos. B. Eng.* **2014**, *61*, 41.
[48] M. R. Moghbeli, M. Shahabi, *Iran Polym. J.* **2011**, *20*, 343.

SUPPORTING INFORMATION

Additional supporting information may be found online in the Supporting Information section at the end of this article.

How to cite this article: Kekevi B, Mert EH. Synthesis of β-myrcene-based macroporous nanocomposite foams: Altering the morphological and mechanical properties by using organo-modified nanoclay. *J Appl Polym Sci*. 2020;e50074. https://doi.org/10.1002/app.50074